
Extracting Visual Facts from Intermediate Layers for Mitigating Hallucinations in Multimodal Large Language Models

Haoran Zhou
Southeast University
haoranzhou0@gmail.com

Zihan Zhang
Southeast University
220242424@seu.edu.cn

Hao Chen*
Southeast University
haochen303@seu.edu.cn

Abstract

Multimodal Large Language Models (MLLMs) have made significant strides by combining visual recognition and language understanding to generate content that is both coherent and contextually accurate. However, MLLMs continue to struggle with object hallucinations, where models produce seemingly plausible but factually incorrect outputs, including objects that do not exist in the image. Recent work has revealed that the prior knowledge in MLLMs significantly suppresses visual information in deep layers, causing hallucinatory outputs. However, how these priors suppress visual information at the intermediate layer stage in MLLMs remains unclear. We observe that visual factual knowledge and the differences between intermediate-layer prior/original probability distributions show similar evolutionary trends in intermediate layers. Motivated by this, we introduce Decoding by Extracting Visual FActs (EVA), a simple, training-free method that dynamically selects intermediate layers with the most significant visual factual information. By contrasting the output distributions of the selected layer derived from the original input and pure-text input, EVA extracts visual factual knowledge and proportionally incorporates it into the final layer to correct the output logits. Importantly, EVA is model-agnostic, seamlessly integrates with various classic decoding strategies, and is applicable across different MLLMs. We validate EVA on widely-used benchmarks, and the results show that it significantly reduces hallucination rates compared to baseline methods, underscoring its effectiveness in mitigating hallucinations.

1 Introduction

Recently, the accelerated advancement of Multimodal Large Language Models (MLLMs) has emerged as a promising trajectory toward realizing Artificial General Intelligence (AGI) [1, 2, 3, 4, 5, 6, 7]. Nevertheless, the practical development of MLLMs is significantly constrained by the persistent challenge of hallucination, a phenomenon wherein models generate assertions about non-existent visual content while omitting critical descriptions of actually present objects, thereby propagating self-deceptive outputs [8, 9, 10, 11, 12]. This issue poses profound risks in high-consequence domains such as medical imaging analysis [13, 14, 15], autonomous driving systems [16, 17], and human-computer interaction [18], where erroneous outputs could lead to irreversible outcomes.

The underlying mechanisms of hallucinations in MLLMs are inherently complex. Unlike prior investigations focused on Large Language Models (LLMs) [19, 20, 21, 22, 23, 24], contemporary research [25, 26] has revealed that MLLMs possess the capacity to encode visual information. Empirical evidence has demonstrated that, to a significant extent, the prior knowledge embedded within

*Corresponding Author.

MLLMs, particularly the textual priors of the LLM serving as the decoder, exerts suppressive effects on visual features in deeper network layers, thereby inducing hallucinatory outputs. Nevertheless, the precise mechanisms through which such priors suppress visual information at the intermediate layer stage in MLLMs remain largely underexplored.

To fill this gap, we leverage the early-exit method [27, 28, 29] to derive next-token probability distributions from intermediate layers for both the original multimodal input (containing visual-textual features) and the pure text input (lacking visual components). We then employ Jensen-Shannon (JS) divergence to quantify the discrepancy between these two distributions for each layer, operationalizing this metric as a measure of how prior knowledge suppresses visual information. Empirical observations reveal that the trend of JS divergence across shallow to deep layers correlates with the probability dynamics of ground-truth tokens (as shown in Figure 2 and Section 3.2). This suggests that **the intermediate layer exhibiting the maximum JS divergence harbors richer visual factual knowledge**. Building on this insight, we introduce the Decoding by Extracting Visual FAct (EVA) method, which identifies visual factual information by contrasting outputs from the selected intermediate layer of the multimodal input with those of the text-only input, thereby correcting hallucinatory outputs during generation. Notably, EVA is training-free and compatible with mainstream decoding strategies, including greedy search, nucleus sampling, and beam search, enabling seamless integration into any MLLM architecture for hallucination mitigation.

Contributions. Our contributions primarily involve investigating how prior knowledge in MLLMs suppresses visual factual knowledge at the intermediate layer stage. We uncovered that visual factual knowledge shares a similar evolutionary trend with the divergence between original and prior probability distributions in intermediate layers. Based on this finding, we propose EVA, a decoding method that refines final outputs by extracting visual factual knowledge from intermediate layers. EVA is seamlessly integrated with four representative MLLMs (InstructBLIP, MiniGPT-4, LLaVA-1.5, and Qwen-VL) using three classic decoding strategies: greedy search, nucleus sampling, and beam search. Experimental results demonstrate that EVA significantly outperforms baselines on visual question answering (VQA) benchmarks (POPE, MME) and achieves superior performance of image captioning datasets.

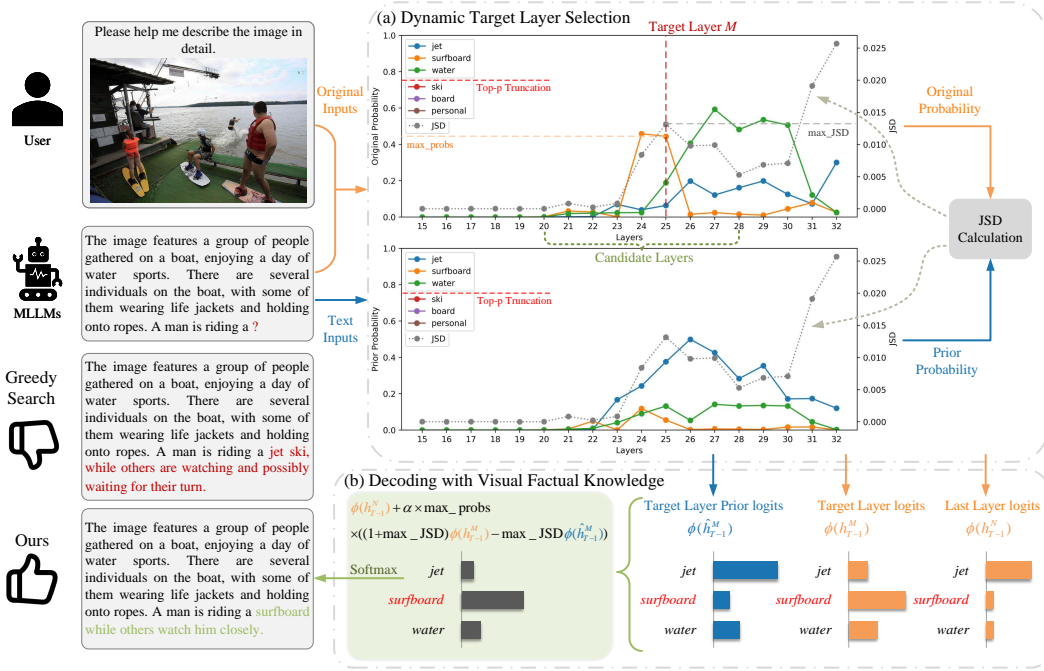


Figure 1: Framework of EVA. (a) Dynamically select an optimal target layer from intermediate layers. (b) Extract visual facts and correct the knowledge in the final layer with visual factual knowledge.

2 Related works

2.1 Causes of Hallucination in MLLMs

Hallucinations are frequently observed in MLLMs when processing visual and textual information. The underlying causes are multifaceted, involving complex interactions and mechanisms across different levels [30]. The inherent differences in feature representation between visual and textual modalities, along with the difficulty of accurate alignment, lead to the attenuation of visual information during cross-modal fusion. This limits the model’s ability to effectively utilize visual signals internally [8, 31]. Additionally, inaccurate image-text matching and biases in training datasets, such as numerous similar images paired with homogenized descriptions, reinforce the model’s reliance on statistical priors [32, 30]. This causes the model to frequently produce "common" but inaccurate answers that do not faithfully correspond to the inputs. Factors such as insufficient cross-modal representation alignment, imbalanced attention allocation, the overshadowing effect of knowledge priors, and hierarchical information attenuation [8, 33] accumulate to make hallucination an unavoidable core challenge in current multimodal models. Moreover, during both model training and inference, strong language priors often suppress or override the perception of visual content, causing the model to favor high-probability linguistic content while ignoring or fabricating objects and attributes absent from the image [32, 31]. Some works [25, 26] have partially validated this point, but the process by which prior knowledge suppresses visual knowledge at the intermediate layer remains unclear.

2.2 Mitigating Hallucination for MLLMs

Recent research on hallucination mitigation in MLLMs has primarily focused on two main avenues: representation optimization during training and decoding strategies. Hallucination Augmented Contrastive Learning [30] introduces hallucinated text as hard negative samples in contrastive learning, strengthening the consistency between non-hallucinatory text and visual representations and improving the model’s ability to distinguish between real and fabricated content. HalluciDoctor [34] tackles hallucination directly at the data source by automatically detecting and removing harmful hallucinatory samples from training data, and balances data distribution through counterfactual sample augmentation, fundamentally enhancing the model’s resistance to hallucination. Additionally, unsupervised decoding and semantic feedback mechanisms such as HELPD [35] and MemVR [36] have been proposed, providing diversified technical solutions for MLLM hallucination mitigation. Collectively, these approaches have significantly enhanced the trustworthiness and robustness of multimodal large models in practical applications. OPERA [37] method introduces an “over-trust penalty” in the decoding combined with a retrospection-allocation mechanism, which dynamically adjusts attention distribution and generation weights. This reduces the model’s over-reliance on a limited set of tokens and better leverages image information without requiring additional training resources. Visual Contrastive Decoding (VCD) [32] is a training-free approach that suppresses hallucinations by contrasting output distributions from original and perturbed visual inputs, thereby reducing dependence on statistical biases and language priors. DeCo [25] adaptively selects the appropriate preceding layers and proportionally integrates knowledge into the final layer to adjust the output logits. Compared with existing decoding methods, our approach can extract visual factual knowledge and integrate it into the final output to mitigate hallucinations.

3 Method

3.1 Preliminary

MLLM generation. MLLMs generally concatenate visual tokens, processed by a visual encoder and projection layer, with embedded textual tokens before feeding them into an autoregressive language model. We denote the visual token sequence as $\mathbf{X}^V = \{x_{v1}, x_{v2}, \dots, x_{vP}\}$ and the textual token sequence as $\mathbf{X}^C = \{x_{c1}, x_{c2}, \dots, x_{cQ}\}$, where P and Q represent the lengths of the visual and textual token sequences, respectively. The final input is thus $\mathbf{X} = \text{concat}(\mathbf{X}^V, \mathbf{X}^C)$. This concatenated input \mathbf{X} is then passed through an MLLM comprising N stacked transformer layers. The intermediate variables generated by the i -th layer, referred to as hidden states, are denoted as $\mathbf{h}^i = \{h_0^i, h_1^i, \dots, h_{T-1}^i\}$, where $T = P + Q$ represents the total sequence length.

During the generation phase, the hidden state at the final position of the last layer is mapped to the vocabulary dimension via an affine layer $\phi(\cdot)$ to predict the probability distribution over next tokens. Formally, this process is expressed as:

$$p(x_T | x_{<T}) = \text{softmax}(\phi(h_{T-1}^N))_{x_T}, x_T \in \mathcal{V} \quad (1)$$

where we use $x_{<T}$ to simplify the sequence $\{x_i\}_{i=0}^{T-1}$ and \mathcal{V} refers to the whole vocabulary set.

3.2 The Intermediate Layers Contain Visual Factual Knowledge

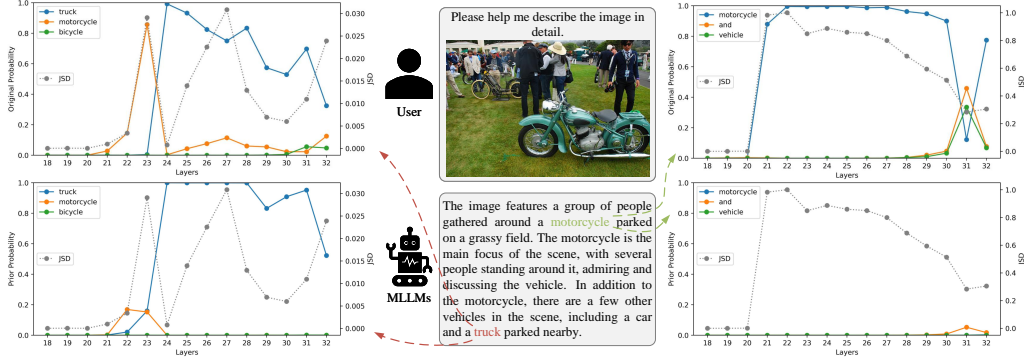


Figure 2: Illustration of the hierarchical evolution trends of hallucinated tokens (red), non-hallucinated tokens (green), and JS divergence values across transformer layers, revealing that non-hallucinated tokens exhibit a trend similar to that of JS divergence values.

Previous works [25, 26] have demonstrated that the representations in the preceding layers effectively capture (to some extent) visual information, while the deep-layer prior knowledge inherent to the Language Model (LLM) component systematically diminishes the likelihood of ground-truth tokens aligned with visual content. We leveraged the early-exit method [27, 28, 29] to derive next-token probability distributions from intermediate layers for both original multimodal inputs (integrating visual and textual features) and text-only inputs (excluding visual components). Leveraging Jensen-Shannon (JS) divergence (detailed in Section 3.3.1), we quantify the dissimilarity between probability distributions of corresponding layers, as a proxy for the degree to which Language Model (LLM) prior knowledge suppresses visual information. This divergence is computed for each intermediate layer to characterize the hierarchical evolution of visual information suppression, from shallow to deep layers, induced by LLM priors.

Figure 2 illustrates this hierarchical evolution with running examples. We analyze the Top-3 tokens ranked by probability in the final layer’s output. For the evolution trend in predicting the non-hallucinated token "motorcycle", both the JS divergence value and the original probability of "motorcycle" sharply increase at the 21st layer, and then decrease at the 31st layer. At the same time, the original probability and prior probability of the hallucinated token "and" both increase at the 31st layer, which indicates that as prior knowledge, "and" suppresses the non-hallucinated token "motorcycle" at the 31st layer. For the evolutionary trajectory in predicting the hallucinated token "truck", both the JS divergence value and the probability of the non-hallucinated token "motorcycle" exhibit an upward trend starting at the 22nd layer, reach a first peak at the 23rd layer, followed by a simultaneous decline to minimum values at the 24th layer, with consistent co-variation thereafter. Concurrently, the original probability and prior probability of the hallucinated token "truck" increase from the 23rd layer, peak at the 24th layer, and then undergo gradual decay. This pattern suggests that the hallucinated token "truck" also acts as prior knowledge to suppress the non-hallucinated token "motorcycle".

Based on the above observations, we hypothesize that intermediate layers with higher JS divergence values contain richer visual factual knowledge, given the similar evolutionary trends between JS divergence values and non-hallucinated tokens. Therefore, we select the intermediate layer with the maximum JS divergence value as the target layer and then contrast its original probability distribution with the prior probability distribution to extract visual factual knowledge.

3.3 Decoding by Extracting Visual Facts from Intermediate Layers

Based on the above hypotheses, we propose Decoding by Extracting Visual Facts (EVA), which can mitigate hallucinations during inference. As depicted in Figure 1, the EVA framework comprises two components: Dynamic Target Layer Selection (Section 3.3.1) and Decoding with Visual Factual Knowledge (Section 3.3.2).

3.3.1 Dynamic Target Layer Selection

Candidate Token Acquisition. Due to the vast vocabulary space, we track only the changes in top-ranked tokens as candidate tokens across different layers to mitigate noise introduced by irrelevant tokens. This approach is grounded in the hypothesis that ground-truth tokens often appear in the top positions of an MLLM’s final-layer output logits [25]. We adopt the truncation strategy proposed in [25] to select candidate tokens, with the default strategy being top- p truncation. Formally:

$$\mathcal{V}_{candidate}(x_T | x_{<T}) = \left\{ x_T \in \mathcal{V} : \sum_{v \in \mathcal{V}_p} P_\tau(x_T = v | x_0, x_1, \dots, x_{T-1}) \leq p \right\} \quad (2)$$

where \mathcal{V} is the whole vocabulary, and p refers to the parameter used in top- p .

Target Layer Selection. We obtain the original probability distribution and prior probability distribution of the intermediate layers with early-exit method. Then, we calculate the JS divergence between the two distributions of the same layer. Formally:

$$d\left(p^j(x_T | x_{<T}), p_{prior}^j(x_T | x_{<T})\right) = \text{JSD}\left(p^j(x_T | x_{<T}) || p_{prior}^j(x_T | x_{<T})\right), x_T \in \mathcal{V}_{candidate} \quad (3)$$

where $\text{JSD}(\cdot, \cdot)$ denotes the Jensen-Shannon divergence. Specifically, $p^j(x_T | x_{<T})$ represents the probability distribution over the next token derived from the original input at the j -th layer, while $p_{prior}^j(x_T | x_{<T})$ signifies the probability distribution over the next token derived from the pure text input at the j -th layer.

Based on the observations in Section 3.2, we identify the target layer by selecting the one with the maximum JS divergence value for extracting visual factual knowledge. Formally, we have:

$$M = \arg \max_{j \in \mathcal{J}} \left\{ \text{JSD}\left(p^j(x_T | x_{<T}) || p_{prior}^j(x_T | x_{<T})\right), x_T \in \mathcal{V}_{candidate} \right\} \quad (4)$$

where $\mathcal{J} \subset \{0, \dots, N-1\}$ is a set of candidate layers.

3.3.2 Decoding with Visual Factual Knowledge.

Dynamic Soft Modulation. Inspired by [25], we introduce two dynamic modulation coefficients, which are initialized as the maximum values of the original probability and the JS divergence from the selected target layer. Formally, we have:

$$\max_prob = \max(\text{softmax}(\phi(h_{T-1}^M))). \quad (5)$$

$$\max_JSD = \text{JSD}\left(p^M(x_T | x_{<T}) || p_{prior}^M(x_T | x_{<T})\right), x_T \in \mathcal{V}_{candidate} \quad (6)$$

Visual Factual Knowledge Guided Decoding. To extract visual factual knowledge, we subtract prior logits from the original logits at the target layer as visual factual knowledge. Subsequently, it is integrated into the original logits of the target layer for soft modulation, and the modulated logits are then proportionally merged into the final layer. We use a hyperparameter α to control the proportion of the extracted visual factual knowledge. By leveraging this knowledge for decoding, the probability of predicting the next token are updated as follows:

$$\tilde{p}(x_T | x_{<T}) = \text{softmax}(\text{logits}) \quad (7)$$

$$\text{logits} = (\phi(h_{T-1}^N)) + \alpha \times \max_prob \times (\phi(h_{T-1}^M) + \max_JSD \times \text{logits}_v), \quad (8)$$

$$\text{logits}_v = \phi(h_{T-1}^M) - \phi(\hat{h}_{T-1}^M) \quad (9)$$

where N is the last layer of MLLM, M is the selected preceding layer, $\phi(\hat{h}_{T-1}^M)$ is the prior logits.

4 Experiments

4.1 Experimental Settings

Baselines. We integrate EVA with diverse decoding strategies including greedy decoding, nucleus sampling, and beam search, and conduct comparative evaluations against multiple baselines for hallucination mitigation as detailed below: Dola [19] is specifically engineered to alleviate hallucinations in factual tasks for LLMs by diminishing shallow semantic interference to enhance the factuality of the final-layer output; VCD [32] mitigates the dominance of language model priors in MLLMs through a subtractive mechanism that generates visual-information-enhanced representations by removing interfering prior knowledge at each sampling step; OPERA [37] employs a dual strategy of dynamically penalizing overconfident tokens based on emerging aggregation patterns and introducing a retrospective allocation mechanism to preemptively address potential hallucinations that have already manifested; DeCo [25] dynamically selects preceding layers and leverages their prior knowledge to rectify final output logits for adjusting prediction biases. For all baselines, default hyperparameters from the original source code are strictly adopted to ensure fair comparability.

Evaluation Models. We select four of the most representative MLLM models for evaluation, including InstructBLIP [38], MiniGPT-4 [39], LLaVA-1.5 [6] and Qwen-VL [40]. All evaluated MLLMs employ a language model size of 7 billion parameters (7B).

Implementation Details. For a 7B-parameter, 32-layer decoder-only architecture language model, we select layers 20–28 as candidates for the preceding layers, following [25]. For the image captioning and VQA tasks, the hyperparameter α is tuned within the range of 0.6 to 5. All experiments are conducted using a single L20 GPU for inference.

4.2 Benchmark and metrics

POPE. The Polling-based Object Probing Evaluation (POPE) [10] is a VQA-based metric designed to assess object hallucination in MLLMs. This framework evaluates hallucinations by posing questions of the form “Is there a <object> in the image?,” where <object> is drawn from three predefined splits: random, popular, and adversarial. The evaluation includes 500 MSCOCO images, with six questions per image for each split. We use the average F1-score computed on random, popular, and adversarial splits.

MME. The comprehensive MLLM Evaluation benchmark (MME) [41] evaluates the perceptual and cognitive capabilities of MLLMs across 14 subtasks, covering domains such as OCR, visual knowledge, attribute relationships, and object recognition.

CHAIR. The Caption Hallucination Assessment with Image Relevance (CHAIR) [42] metric, widely adopted in image captioning tasks, detects hallucinated objects by comparing extracted objects against ground-truth labels and evaluates hallucination at both the instance level (CHAIR_I) and sentence level (CHAIR_S), as formalized in Eq. 10. Following the experimental protocol in [37], we use consistent settings: 500 images from the MSCOCO 2014 validation dataset and the fixed prompt “Please help me describe the image in detail.” for evaluation.

$$\text{CHAIR}_I = \frac{|\{\text{hallucinated objects}\}|}{\text{all mentioned objects}}, \text{CHAIR}_S = \frac{|\{\text{captions with hallucinated objects}\}|}{\text{all captions}}. \quad (10)$$

4.3 Experimental Results

Results on POPE. The experimental results on the POPE benchmark under random, popular, and adversarial settings are summarized in Table 1. A prominent observation is the consistent and robust performance of our proposed EVA method. Across different sampling scenarios, EVA consistently achieves improved F1-scores compared to baseline methods on all evaluated MLLMs, with the most notable improvement reaching 21.9 points under the nucleus decoding setting for MiniGPT-4. Moreover, EVA generally outperforms competing methods such as DoLa, DeCo, OPERA, and VCD, demonstrating its superior capability in suppressing hallucinations. EVA outperforms DeCo possibly because DeCo merely selects the layer with the maximum probability from intermediate layers, without considering that the maximum probability may be influenced by prior probability interference

(as shown in Figure 2). This oversight leads to the selection of incorrect visual information for correcting the final output. In conclusion, the performance gain highlights EVA’s effectiveness in mitigating object hallucinations by extracting visual factual knowledge.

Table 1: POPE hallucination evaluation results. The best results are in bold.

Decoding	Method	InstructBLIP F1 ↑	MiniGPT-4 F1 ↑	LLaVA-1.5 F1 ↑	Qwen-VL F1 ↑
Greedy	Vanilla	80.0	58.5	82.2	85.2
	DoLa	83.4	72.8	83.2	85.8
	DeCo	84.9	77.4	86.7	86.3
	EVA (Ours)	85.2 ↑5.2	78.2 ↑19.7	87.1 ↑4.9	86.3 ↑1.1
Beam Search	Vanilla	84.4	70.3	84.9	85.3
	OPERA	84.8	73.3	85.4	86.1
	DeCo	84.9	77.9	86.7	86.4
	EVA (Ours)	85.0 ↑0.6	78.0 ↑7.7	87.1 ↑2.2	86.2 ↑0.9
Nucleus	Vanilla	79.8	52.8	83.1	84.5
	VCD	79.9	56.0	83.1	84.7
	DeCo	81.8	63.8	85.4	85.2
	EVA (Ours)	84.5 ↑4.7	74.7 ↑21.9	87.4 ↑4.3	85.4 ↑0.9

Results on MME Hallucination Subset. The evaluation on the MME subset extends beyond the scope of POPE, encompassing hallucination issues at both object and attribute levels. Results in Table 2 demonstrate that the EVA method yields overall positive effects on object-level metrics, contributing to significant improvements in overall performance. Although EVA’s total score on the InstructBLIP model does not achieve the highest value (slightly below VCD’s 447.67), it attains the highest total scores on other models, reflecting its effectiveness and stability in enhancing hallucination mitigation across MLLMs. These improvements highlight the importance of EVA’s effective utilization of visual information, thereby exerting a positive impact on a broader range of hallucination challenges.

Table 2: Results on the hallucination subset of MME with nucleus sampling. The best results within each setting are bolded.

Model	Decoding	Object-level		Attribute-level		Total Scores↑
		Existence↑	Count↑	Position↑	Color↑	
LLaVA-1.5	Nucleus	175.67	124.67	114.00	151.00	565.33
	VCD	184.66	138.33	128.67	153.00	604.66
	DeCo	190.00	148.33	115.00	165.00	618.33
	Ours	190.00 ↑14.33	158.33 ↑33.66	133.33 ↑19.33	170.00 ↑19.00	651.67 ↑86.34
Qwen-VL	Nucleus	155.00	127.67	131.67	173.00	587.33
	VCD	156.00	131.00	128.00	181.67	596.67
	DeCo	185.00	135.00	106.67	175.00	601.67
	Ours	175.00 ↑20.00	135.00 ↑7.33	115.00 ↓16.67	185.00 ↑12.00	610.00 ↑22.67
InstructBLIP	Nucleus	141.00	75.33	66.67	97.33	380.33
	VCD	168.33	92.33	64.00	123.00	447.67
	DeCo	185.00	55.00	48.33	100.00	388.33
	Ours	185.00 ↑44.00	60.00 ↓15.33	55.00 ↓11.67	115.00 ↑17.67	415.00 ↑34.67
MiniGPT-4	Nucleus	65.00	70.00	46.67	56.67	238.33
	VCD	105.00	61.67	68.33	85.00	320.00
	DeCo	75.00	70.00	53.33	65.00	263.33
	Ours	103.33 ↑38.33	78.33 ↑8.33	75.00 ↑28.33	65.00 ↑8.33	321.67 ↑83.34

Results on MME Hallucination Full Set. As illustrated in Figure 3, we also evaluate EVA on the MME Full Set to assess its impact on the overall capabilities of MLLMs. Given the comparable performance trends across all models, we present results for LLaVA-1.5 as a representative case. The application of EVA leads to substantial improvements in perception-based tasks. However, this is accompanied by a reduction in the original recognition capabilities of MLLMs, which may be attributed to EVA’s mechanism of subtracting LLM priors, thereby causing a decline in recognition capabilities.

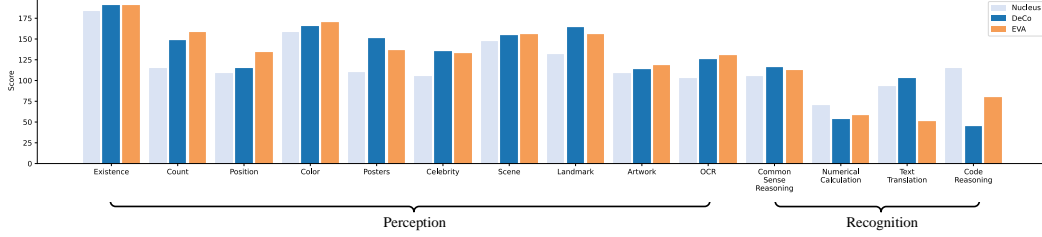


Figure 3: MME full set results on LLaVA-1.5 with nucleus sampling. EVA leads to substantial enhancement in LVLMS’ perception capacities.

Results on CHAIR. From Table 3, we observe that EVA predominantly outperforms other approaches in mitigating hallucinations across four MLLMs. The proposed EVA approach effectively reduces hallucinations in visual description tasks through the extraction of visual factual knowledge.

Table 3: CHAIR hallucination evaluation results. Lower scores indicate fewer hallucinations. The best results are in bold. *Qwen-VL may generate relatively short sentences leading to excessively low results. Note that we use the baseline’s original decoding settings for a fair comparison and run EVA under the same settings.

Decoding	Method	InstructBLIP		MiniGPT-4		LLaVA-1.5		Qwen-VL	
		CHAIR _S ↓	CHAIR _I ↓						
Greedy	Vanilla	58.8	23.7	31.8	9.9	45.0	14.7	46.0	12.5
	DoLa	48.4	15.9	32.2	10.0	47.8	13.8	46.8	12.9
	DeCo	41.2	14.4	27.0	8.8	37.8	11.1	42.2	10.7
	EVA (Ours)	41.2 ↓17.6	13.0 ↓10.7	26.0 ↓5.8	9.2 ↓0.7	35.6 ↓9.4	11.3 ↓3.4	6.8 ↓39.2	4.4 ↓8.1
Beam Search	Vanilla	55.6	15.8	30.6	9.5	48.8	13.9	41.8	10.8
	OPERA	46.4	14.2	26.2	9.5	44.6	12.8	34.6	9.5
	DeCo	43.8	12.7	24.8	7.5	33.0	9.7	32.0	8.7
	EVA (Ours)	40.6 ↓15.0	12.2 ↓3.6	22.6 ↓8.0	8.0 ↓1.5	37.4 ↓11.4	11.0 ↓2.9	2.8 ↓39.0	2.0 ↓8.8
Nucleus	Vanilla	54.6	24.8	32.6	10.7	48.8	14.2	49.2	13.1
	VCD	58.0	17.0	33.8	11.1	54.0	16.0	46.4	11.9
	DeCo	43.6	12.9	30.8	9.5	42.8	13.2	43.8	11.8
	EVA (Ours)	39.0 ↓15.6	15.0 ↓9.8	26.0 ↓6.6	10.1 ↓0.6	40.0 ↓8.8	11.4 ↓2.8	7.4 ↓41.8	4.1 ↓9.0

4.4 Discussions

Effectiveness of Visual Knowledge Extraction. To validate the effectiveness of our approach, we conduct an experiment comparing our visual knowledge extraction method with DeCo [25]. Following [25], we randomly sample 500 images from the MSCOCO dataset and use prompts to elicit raw responses from LLaVA1.5-7B. We then extract all non-existent objects mentioned in the responses, along with their preceding contextual text, and feed this data into the MLLM. We observe the next-token probabilities at the selected layer to derive candidate tokens, denoted as $\mathcal{V}_{candidate}$, with a default confidence threshold of 0.9. We then label the tokens in $\mathcal{V}_{candidate}$. Specifically, we filter out data where $\mathcal{V}_{candidate}$ contains at least one ground truth token and observe whether an activated ground truth token exists among the candidate tokens, formally expressed as:

$$\exists x_a \in \mathcal{V}_{candidate}, p(x_a | x_{<s}) - p(x_h | x_{<s}) > 0 \quad (11)$$

where x_a denotes the activated ground-truth token, and x_h represents the token with the highest probability of being a hallucinated token in the probability distribution of the final layer. Additionally, we count the total number of activated ground truth token. Based on the experimental setup described above, we compare the statistical results derived from the following two probabilities:

$$p_v(\cdot | x_{<s}) = \text{softmax}(\phi(h_{T-1}^M) - \phi(\hat{h}_{T-1}^M)), \quad (12)$$

$$p_d(\cdot | x_{<s}) = \text{softmax}(\phi(h_{T-1}^A)), \quad (13)$$

$$\mathcal{A} = \arg \max_{j \in \mathcal{J}} \{p^j(x_T | x_{<T}), x_T \in \mathcal{V}_{candidate}\} \quad (14)$$

where h_{T-1}^A is the hidden state of the target layer selected by DeCo [25] method, $p_v(\cdot | x_{<s})$ represents the probability distribution of visual knowledge extracted by our method, while $p_d(\cdot | x_{<s})$ denotes that of DeCo[25].

Table 4: Statistical results obtained from ours and DeCo [25].

Method	Number of Data	Number of Token
DeCo	157	259
Ours	170	302

As shown in Table 4, the statistical results demonstrate that our method yields a larger quantity of data containing at least one ground truth token and a higher count of activated ground truth tokens. This suggests that our method is more effective in extracting visual factual knowledge.

Case Study on LLaVA-Bench. Figure 4 presents two illustrative case studies demonstrating that, given identical prompts and images, conventional decoding methods often produce object hallucinations driven by inherent statistical biases and language priors acquired during pretraining. Specifically, the examples reveal hallucinated objects such as “clock,” “handbag,” and “bottle,” which frequently co-occur with the true context object “room.” In contrast, our proposed EVA method effectively mitigates these hallucination artifacts while maintaining the coherence and informativeness of the generated text. This highlights EVA’s ability to dynamically incorporate visual factual knowledge, resulting in more accurate and reliable multimodal outputs

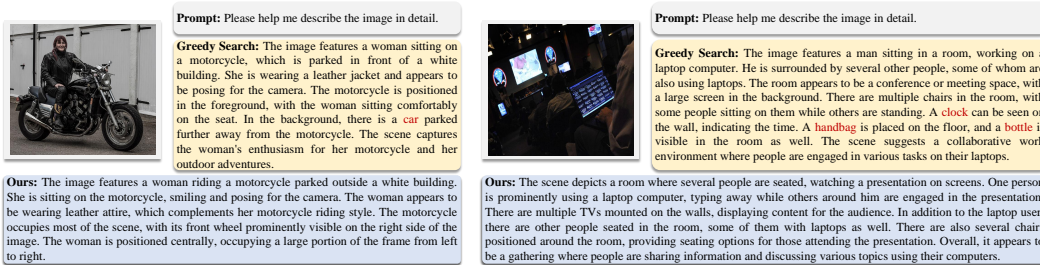


Figure 4: Illustration of hallucination correction by EVA with two samples from LLaVA-Bench. Hallucinated objects from LLaVA’s greedy search are highlighted in red.

5 Conclusion and Limitation

In this paper, we investigate how prior knowledge in MLLMs suppresses visual factual knowledge at the intermediate layer stage. We find that visual factual knowledge exhibits an evolutionary trend analogous to the divergence between raw probability distributions and prior probability distributions in intermediate layers. Based on this finding, we propose EVA, a train-free decoding method that revises final outputs by extracting visual factual knowledge from intermediate layers. We validated EVA on widely used benchmarks, and the results show that compared with baseline methods, EVA significantly reduces the incidence of hallucinations, highlighting its effectiveness in mitigating hallucinations.

Limitation. Due to GPU cost constraints, our experiments are exclusively conducted on a limited set of MLLMs, without exploring additional models or those with larger parameter scales.

References

- [1] P. Wang, S. Bai, S. Tan, S. Wang, Z. Fan, J. Bai, K. Chen, X. Liu, J. Wang, W. Ge *et al.*, “Qwen2-vl: Enhancing vision-language model’s perception of the world at any resolution,” *arXiv preprint arXiv:2409.12191*, 2024.
- [2] Y. Yao, T. Yu, A. Zhang, C. Wang, J. Cui, H. Zhu, T. Cai, H. Li, W. Zhao, Z. He *et al.*, “Minicpm-v: A gpt-4v level mllm on your phone,” *arXiv preprint arXiv:2408.01800*, 2024.
- [3] H. Lu, W. Liu, B. Zhang, B. Wang, K. Dong, B. Liu, J. Sun, T. Ren, Z. Li, H. Yang *et al.*, “Deepseek-vl: towards real-world vision-language understanding,” *arXiv preprint arXiv:2403.05525*, 2024.
- [4] C. Team, “Chameleon: Mixed-modal early-fusion foundation models,” *arXiv preprint arXiv:2405.09818*, 2024.
- [5] J. Achiam, S. Adler, S. Agarwal, L. Ahmad, I. Akkaya, F. L. Aleman, D. Almeida, J. Altenschmidt, S. Altman, S. Anadkat *et al.*, “Gpt-4 technical report,” *arXiv preprint arXiv:2303.08774*, 2023.
- [6] H. Liu, C. Li, Y. Li, and Y. J. Lee, “Improved baselines with visual instruction tuning,” in *Proceedings of the IEEE/CVF Conference on Computer Vision and Pattern Recognition*, 2024, pp. 26 296–26 306.
- [7] E. Chern, J. Su, Y. Ma, and P. Liu, “Anole: An open, autoregressive, native large multimodal models for interleaved image-text generation,” *arXiv preprint arXiv:2407.06135*, 2024.
- [8] Z. Bai, P. Wang, T. Xiao, T. He, Z. Han, Z. Zhang, and M. Z. Shou, “Hallucination of multimodal large language models: A survey,” *arXiv preprint arXiv:2404.18930*, 2024.
- [9] H. Liu, W. Xue, Y. Chen, D. Chen, X. Zhao, K. Wang, L. Hou, R. Li, and W. Peng, “A survey on hallucination in large vision-language models,” *arXiv preprint arXiv:2402.00253*, 2024.
- [10] Y. Li, Y. Du, K. Zhou, J. Wang, W. X. Zhao, and J.-R. Wen, “Evaluating object hallucination in large vision-language models,” *arXiv preprint arXiv:2305.10355*, 2023.
- [11] F. Liu, K. Lin, L. Li, J. Wang, Y. Yacoob, and L. Wang, “Mitigating hallucination in large multi-modal models via robust instruction tuning,” *arXiv preprint arXiv:2306.14565*, 2023.
- [12] V. Rawte, A. Sheth, and A. Das, “A survey of hallucination in large foundation models,” *arXiv preprint arXiv:2309.05922*, 2023.
- [13] J. Chen, C. Gui, R. Ouyang, A. Gao, S. Chen, G. H. Chen, X. Wang, R. Zhang, Z. Cai, K. Ji *et al.*, “Huatuogpt-vision, towards injecting medical visual knowledge into multimodal llms at scale,” *arXiv preprint arXiv:2406.19280*, 2024.
- [14] M. Hu, S. Pan, Y. Li, and X. Yang, “Advancing medical imaging with language models: A journey from n-grams to chatgpt,” *arXiv preprint arXiv:2304.04920*, 2023.
- [15] S. Wang, Z. Zhao, X. Ouyang, Q. Wang, and D. Shen, “Chatcad: Interactive computer-aided diagnosis on medical image using large language models,” *arXiv preprint arXiv:2302.07257*, 2023.
- [16] C. Cui, Y. Ma, X. Cao, W. Ye, Y. Zhou, K. Liang, J. Chen, J. Lu, Z. Yang, K.-D. Liao *et al.*, “A survey on multimodal large language models for autonomous driving,” in *Proceedings of the IEEE/CVF Winter Conference on Applications of Computer Vision*, 2024, pp. 958–979.
- [17] W. Wang, J. Xie, C. Hu, H. Zou, J. Fan, W. Tong, Y. Wen, S. Wu, H. Deng, Z. Li *et al.*, “Drivemlm: Aligning multi-modal large language models with behavioral planning states for autonomous driving,” *arXiv preprint arXiv:2312.09245*, 2023.
- [18] P. Brie, N. Burny, A. Sluÿters, and J. Vanderdonckt, “Evaluating a large language model on searching for gui layouts,” *Proceedings of the ACM on Human-Computer Interaction*, vol. 7, no. EICS, pp. 1–37, 2023.
- [19] Y.-S. Chuang, Y. Xie, H. Luo, Y. Kim, J. Glass, and P. He, “Dola: Decoding by contrasting layers improves factuality in large language models,” *arXiv preprint arXiv:2309.03883*, 2023.
- [20] S. Chen, M. Xiong, J. Liu, Z. Wu, T. Xiao, S. Gao, and J. He, “In-context sharpness as alerts: An inner representation perspective for hallucination mitigation,” *arXiv preprint arXiv:2403.01548*, 2024.

- [21] H. Orgad, M. Toker, Z. Gekhman, R. Reichart, I. Szpektor, H. Kotek, and Y. Belinkov, “Llms know more than they show: On the intrinsic representation of llm hallucinations,” *arXiv preprint arXiv:2410.02707*, 2024.
- [22] T. Chen, Z. Tan, T. Gong, Y. Wu, Q. Chu, B. Liu, J. Ye, and N. Yu, “Llama slayer 8b: Shallow layers hold the key to knowledge injection,” *arXiv preprint arXiv:2410.02330*, 2024.
- [23] T. Lu, M. Gao, K. Yu, A. Byerly, and D. Khashabi, “Insights into llm long-context failures: When transformers know but don’t tell,” *arXiv preprint arXiv:2406.14673*, 2024.
- [24] M. Wang, Y. Yao, Z. Xu, S. Qiao, S. Deng, P. Wang, X. Chen, J.-C. Gu, Y. Jiang, P. Xie *et al.*, “Knowledge mechanisms in large language models: A survey and perspective,” *arXiv preprint arXiv:2407.15017*, 2024.
- [25] C. Wang, X. Chen, N. Zhang, B. Tian, H. Xu, S. Deng, and H. Chen, “Mllm can see? dynamic correction decoding for hallucination mitigation,” *arXiv preprint arXiv:2410.11779*, 2024.
- [26] Y. Liang, Z. Cai, J. Xu, G. Huang, Y. Wang, X. Liang, J. Liu, Z. Li, J. Wang, and S.-L. Huang, “Unleashing region understanding in intermediate layers for mllm-based referring expression generation,” *Advances in Neural Information Processing Systems*, vol. 37, pp. 120 578–120 601, 2024.
- [27] S. Teerapittayanon, B. McDanel, and H.-T. Kung, “Branchynet: Fast inference via early exiting from deep neural networks,” in *2016 23rd international conference on pattern recognition (ICPR)*. IEEE, 2016, pp. 2464–2469.
- [28] M. Elbayad, J. Gu, E. Grave, and M. Auli, “Depth-adaptive transformer,” *arXiv preprint arXiv:1910.10073*, 2019.
- [29] T. Schuster, A. Fisch, J. Gupta, M. Dehghani, D. Bahri, V. Tran, Y. Tay, and D. Metzler, “Confident adaptive language modeling,” *Advances in Neural Information Processing Systems*, vol. 35, pp. 17 456–17 472, 2022.
- [30] C. Jiang, H. Xu, M. Dong, J. Chen, W. Ye, M. Yan, Q. Ye, J. Zhang, F. Huang, and S. Zhang, “Hallucination augmented contrastive learning for multimodal large language model,” in *Proceedings of the IEEE/CVF Conference on Computer Vision and Pattern Recognition*, 2024, pp. 27 036–27 046.
- [31] Y.-L. Lee, Y.-H. Tsai, and W.-C. Chiu, “Delve into visual contrastive decoding for hallucination mitigation of large vision-language models,” *arXiv preprint arXiv:2412.06775*, 2024.
- [32] S. Leng, H. Zhang, G. Chen, X. Li, S. Lu, C. Miao, and L. Bing, “Mitigating object hallucinations in large vision-language models through visual contrastive decoding,” in *Proceedings of the IEEE/CVF Conference on Computer Vision and Pattern Recognition*, 2024, pp. 13 872–13 882.
- [33] Y. Wang, M. Zhang, J. Sun, C. Wang, M. Yang, H. Xue, J. Tao, R. Duan, and J. Liu, “Mirage in the eyes: Hallucination attack on multi-modal large language models with only attention sink,” *arXiv preprint arXiv:2501.15269*, 2025.
- [34] Q. Yu, J. Li, L. Wei, L. Pang, W. Ye, B. Qin, S. Tang, Q. Tian, and Y. Zhuang, “Hallucidoctor: Mitigating hallucinatory toxicity in visual instruction data,” in *Proceedings of the IEEE/CVF Conference on Computer Vision and Pattern Recognition*, 2024, pp. 12 944–12 953.
- [35] X. Zou, Y. Wang, Y. Yan, S. Huang, K. Zheng, J. Chen, C. Tang, and X. Hu, “Look twice before you answer: Memory-space visual retracing for hallucination mitigation in multimodal large language models,” *arXiv preprint arXiv:2410.03577*, 2024.
- [36] F. Yuan, C. Qin, X. Xu, and P. Li, “Helpd: Mitigating hallucination of lvlms by hierarchical feedback learning with vision-enhanced penalty decoding,” *arXiv preprint arXiv:2409.20429*, 2024.
- [37] Q. Huang, X. Dong, P. Zhang, B. Wang, C. He, J. Wang, D. Lin, W. Zhang, and N. Yu, “Opera: Alleviating hallucination in multi-modal large language models via over-trust penalty and retrospection-allocation,” in *Proceedings of the IEEE/CVF Conference on Computer Vision and Pattern Recognition*, 2024, pp. 13 418–13 427.
- [38] W. Dai, J. Li, D. LI, A. Tiong, J. Zhao, W. Wang, B. Li, P. N. Fung, and S. Hoi, “Instructblip: Towards general-purpose vision-language models with instruction tuning,” in *Advances in Neural Information Processing Systems*, A. Oh, T. Naumann, A. Globerson, K. Saenko, M. Hardt, and S. Levine, Eds., vol. 36. Curran Associates, Inc., 2023, pp.

- 49 250–49 267. [Online]. Available: https://proceedings.neurips.cc/paper_files/paper/2023/file/9a6a435e75419a836fe47ab6793623e6-Paper-Conference.pdf
- [39] D. Zhu, J. Chen, X. Shen, X. Li, and M. Elhoseiny, “MiniGPT-4: Enhancing vision-language understanding with advanced large language models,” in *The Twelfth International Conference on Learning Representations*, 2024. [Online]. Available: <https://openreview.net/forum?id=1tZbq88f27>
- [40] J. Bai, S. Bai, Y. Chu, Z. Cui, K. Dang, X. Deng, Y. Fan, W. Ge, Y. Han, F. Huang *et al.*, “Qwen technical report,” *arXiv preprint arXiv:2309.16609*, 2023.
- [41] C. Fu, Y.-F. Zhang, S. Yin, B. Li, X. Fang, S. Zhao, H. Duan, X. Sun, Z. Liu, L. Wang *et al.*, “Mme-survey: A comprehensive survey on evaluation of multimodal llms,” *arXiv preprint arXiv:2411.15296*, 2024.
- [42] A. Rohrbach, L. A. Hendricks, K. Burns, T. Darrell, and K. Saenko, “Object hallucination in image captioning,” *arXiv preprint arXiv:1809.02156*, 2018.

Appendix

A Ablation Results of Dynamic Soft Modulation

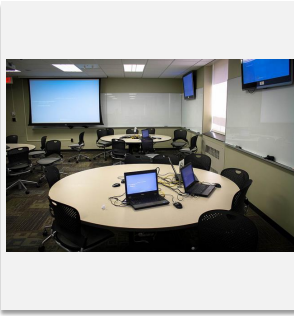
To quantify the effect of soft modulation, we evaluated the results of removing the "max_JSD", removing the "max_prob", and removing both with greedy search. The ablation results are shown in Table 5.

Table 5: Ablation study of soft modulation.

Method	MiniGPT-4 F1 ↑	Qwen-VL F1 ↑
EVA	78.2	86.3
EVA(w/o max_JSD)	77.8	86.1
EVA(w/o max_prob)	76.9	84.6
EVA(w/o max_JSD & max_prob)	76.6	84.5

B Case Studies across Diverse MLLMs

Additional case studies across diverse MLLMs are provided to demonstrate the effectiveness of EVA. Specifically, Figures 5, 6, 7, and 8 respectively present further instances of hallucination corrections by our method for InstructBLIP, MiniGPT-4, LLaVA-1.5, and Qwen-VL.



Prompt: Please help me describe the image in detail.

InstructBLIP (Greedy): The image depicts a large conference room with a round table in the center. The table is surrounded by several chairs, with a total of 12 chairs arranged around it. There are also two laptops placed on the table, one on the left side and the other on the right side. A projector screen is mounted on the wall, providing a visual aid for the meeting or presentation taking place in the room. A television is also visible on the left side of the room, likely used for additional visual support. **A remote control can be seen on the table, possibly used to control the projector or other equipment in the room.**

InstructBLIP (Ours): The scene depicts a room with tables and chairs arranged around a large white round table. There are several lap computers placed on top of the table, ready for use. Additionally, there are several other lap computers scattered around the room, ready to be utilized. A monitor hangs above the table, likely used for projecting presentations or other visual content during meetings or classes. There are several chairs positioned around the table and around the room, providing seating for the laptop users.

Prompt: Please help me describe the image in detail.

InstructBLIP (Beam Search): The image features a large, rectangular pizza sitting on a wooden cutting board on a dining table. The pizza is topped with tomato sauce and cheese, and it appears to be freshly baked. The pizza is placed in the center of the table, making it the focal point of the dining area. There are several chairs placed around the table, suggesting that the pizza is meant to be shared among a group of people. **In addition to the pizza, there are a few utensils placed on the table, such as a fork and a knife, suggesting that the pizza is ready to be enjoyed.**



InstructBLIP (Ours): The image depicts a large pizza sitting on top of a wooden table. The pizza is rectangular in shape and appears to be freshly cooked, judging by its appearance and texture. The pizza is placed on top of a board or cutting board, ready to be served or eaten. There are two chairs visible in the background of the table, one on the left side and another on the right side, ready for diners to sit down and enjoy the delicious pizza.

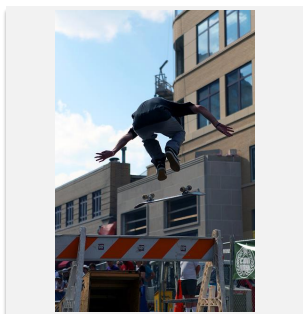


Prompt: Please help me describe the image in detail.

InstructBLIP (Nucleus): The image features a medium-sized yellow cat lying on a couch. The cat appears to be stretching or resting its head, relaxing on the furniture. There are various cushions throughout the scene, including several cushions placed on the backrest of the couch, a few on the armrests, and a few scattered on the floor. The cushions add texture and depth to the image, making it more visually appealing. **Additionally, a remote control can be seen placed on the left-hand side of the scene, possibly providing entertainment for the cat.**

InstructBLIP (Ours): The image depicts an orange cat lying on a gray chair, resting on its side. The cat is lying down on the chair with its eyes closed, its body relaxed and its tail curled upwards. The cat appears to be content and contentedly resting on the chair.

Figure 5: EVA's performance in mitigating hallucinations of InstructBLIP on three decoying methods. Hallucinated content is highlighted in red.



Prompt: Please help me describe the image in detail.

MiniGPT-4 (Greedy): This image shows a person riding a skateboard over a ramp. The person is wearing a black shirt and black pants, and **has a black backpack on their back**. The ramp is made of wood and has a metal railing on either side. There are several people in the background watching the skateboarder. The image is taken from a high angle, looking down at the skateboarder from above. The sky is blue and there are a few clouds in the background.

MiniGPT-4 (Ours): This image depicts a man riding a skateboard over a ramp. He is wearing a black shirt and black pants, and has black shoes on his feet. The background of the image shows a group of people standing around a street corner, watching the skateboarder perform his trick. There are buildings in the background, including one with windows on the upper floor.

Prompt: Please help me describe the image in detail.

MiniGPT-4 (Beam Search): The image shows a blue and white fire hydrant in front of a brick building. The hydrant is decorated with a mural of a cityscape, **including a train station, a skyscraper, and a park**. The mural appears to be painted on the surface of the hydrant itself, rather than being attached to it.



MiniGPT-4 (Ours): This image depicts a blue fire hydrant with white and black paintings on it, depicting a building with windows and doors. The background is a sidewalk with pavers and trees in the distance.



Prompt: Please help me describe the image in detail.

MiniGPT-4 (Nucleus): This image shows a bedroom with a bed, chairs, and a table. The walls are striped and there is a fireplace in the corner of the room. The room is dimly lit with candles on the table and chairs. There is a rug on the floor and **a vase of flowers on the table**.

MiniGPT-4 (Ours): This image depicts a room with stripes on the walls and ceiling, and a fireplace in the corner of the room. There are tables and chairs in the room, and a rug on the floor.

Figure 6: EVA’s performance in mitigating hallucinations of MiniGPT-4 on three decoying methods. Hallucinated content is highlighted in red.



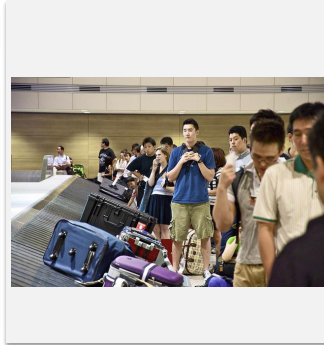
Prompt: Please help me describe the image in detail.

LLaVA-1.5 (Greedy): The image captures a baseball game in progress, with a young boy swinging a baseball bat at a ball. The boy is wearing a baseball uniform and is in the middle of his swing. The sports ball is visible in the air, close to the boy. There are several other people in the scene, including teammates and opponents. Some of them are standing near the boy, while others are positioned further away. A baseball glove can be seen on the right side of the image, likely belonging to one of the players. **In the background, there are a few chairs and a bench, possibly for spectators or resting players.**

LLaVA-1.5 (Ours): The scene depicts a baseball game taking place on a field with players actively participating. There are two main players visible: one batter swinging his baseball bat at an incoming ball, and another player positioned behind him, ready to catch it if necessary. Other players can be seen scattered around the field, either preparing for their turn or awaiting their turn to bat or field. There are also spectators present in the background, cheering and watching the game unfold. Various equipment items such as a baseball glove can be seen on the field as well, ready for use during the game.

Prompt: Please help me describe the image in detail.

LLaVA-1.5 (Beam Search): The image depicts a large group of people gathered in an airport terminal, waiting for their luggage. There are at least 13 people visible in the scene, with some standing closer to the foreground and others further in the background. Various pieces of luggage can be seen throughout the scene, including suitcases, backpacks, and handbags. There are at least 7 suitcases, 3 backpacks, and 4 handbags scattered around the area. Some of the suitcases and backpacks are placed on the ground, while others are being held by the people in the crowd. **In addition to the luggage, a tennis racket can be spotted in the middle of the scene, possibly belonging to one of the travelers.**



LLaVA-1.5 (Ours): The scene depicts a crowded airport terminal where many people are waiting in line with their luggage. There are at least thirteen people visible in the image, each with different luggage items such as suitcases and backpacks. Some suitcases can be seen placed on the floor while others are placed next to their owners. There are several suitcases positioned throughout the scene, including ones near the center of the line, towards the right side of the terminal, and others towards the left side. Backpacks can also be seen placed near some of the waiting passengers, further adding to the crowded atmosphere of the scene.

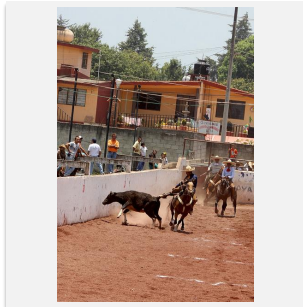


Prompt: Please help me describe the image in detail.

LLaVA-1.5 (Nucleus): The image features an orange road sign, indicating that construction is ahead. The sign is sitting on a pole at the edge of a sidewalk. Several cars are visible in the scene, some parked and others moving through the intersection. In addition to the vehicles, there are numerous pedestrians scattered around the area, some close to the street, and others further back on the sidewalk. Two trucks are present as well, one located closer to the front left of the scene and the other further back on the right side. **This busy urban setting includes a stop sign and a fire hydrant near the sidewalk.**

LLaVA-1.5 (Ours): The scene depicts an orange obstruct construction sign placed on a street corner next to the road. The sign is positioned on a green pole, drawing attention to the construction site ahead. There are several cars parked or driving by on the street, including one car parked directly behind the sign. There are also several other cars scattered along the street, indicating traffic flowing past the construction site. Additionally, two trucks are visible on the street, one towards the left side of the scene and another near the right edge of the image.

Figure 7: EVA's performance in mitigating hallucinations of LLaVA-1.5 on three decoying methods. Hallucinated content is highlighted in red.



Prompt: Please help me describe the image in detail.

Qwen-VL (Greedy): The scene takes place in a courtyard where a group of men are chasing a cow. There are two men on horses in the middle of the scene, one on the left and one on the right, both appear to be holding lassos. They are chasing the cow, which is running towards the left side of the scene. There are several other people in the scene, some on foot, others on horses. One person on the right side of the image is riding a horse without a rider. **In the background, there are two cars parked, one near the center and the other towards the right side of the image.** The courtyard is fenced in, with the cow running towards a gate in the middle of the fence.

Qwen-VL (Ours): The scene takes place at a rodeo where a man on horseback is trying to wrangle a black and white cow. The cow is running in one direction while the man on horseback and his horse are running in the opposite direction. There are several people present, some of them riding horses, while others are on foot. One person is holding onto the cow's tail, while others are watching the man try to wrangle the cow. The people are spread out throughout the area, with some being closer to the action and others watching from a distance. Overall, it seems like an exciting and action-packed moment at the rodeo.

Prompt: Please help me describe the image in detail.

Qwen-VL (Beam Search): The image shows a group of medical professionals gathered in a room. They appear to be wearing scrubs and are focused on a large piece of medical equipment, which occupies a significant portion of the room. The doctors and nurses are standing around the equipment, likely observing or preparing it for use in an upcoming procedure. In addition to the medical staff and the large machine, the room also **contains several chairs, a keyboard, and a laptop. There are also two clocks on the wall, one near the top and another closer to the bottom, providing the time for the medical team.**



Qwen-VL (Ours): In a room full of people wearing blue scrubs, one man is sitting down and wearing a headset. He is sitting next to a large piece of equipment with many screens and controls. There are other people nearby, some standing closer to the equipment, while others are further away in the room. The man with the headset seems to be the focus of the scene as he operates the complex machinery.



Prompt: Please help me describe the image in detail.

Qwen-VL (Nucleus): A cat is laying on a desk in front of a computer **with a mouse** and a keyboard. There is also a laptop and a monitor in the scene, and a cup.

Qwen-VL (Ours): A tabby cat laying on a desk next to two computers, a laptop and a monitor.

Figure 8: EVA's performance in mitigating hallucinations of Qwen-VL on three decoing methods. Hallucinated content is highlighted in red.